Turbulence modulation by settling inertial aerosols in Eulerian-Eulerian and Eulerian-Lagrangian simulations of homogeneously sheared turbulence

M. Houssem Kasbaoui [*]

School for Engineering of Matter, Transport and Energy, Arizona State University,
Tempe, Arizona 85281, USA

Settling inertial aerosols dispersed at high enough concentration modulate the structure of the suspending turbulent flow. The present study addresses this modulation in a canonical flow, which is homogeneously sheared turbulence (HST). Eulerian-Eulerian (EE) and Eulerian-Lagrangian (EL) simulations are conducted in the semidilute regime, i.e., such that the particulate phase is sufficiently dilute to neglect particle-particle interaction but sufficiently concentrated to be strongly coupled with the carrier flow. Four cases are considered for which the Stokes number based on the Kolmogorov timescale is $St_\eta = 0.06$ or 0.19 and mass loading is $M = 0.125$ or 0.5. Turbulence is initialized with a Taylor microscale Reynolds number $Re_{\lambda,0} = 29$ and is strongly sheared, resulting in a shear number $S_0^* = 27$. Simulations of the suspension with $St_\eta = 0.06$ and $M = 0.125$ show no turbulence modification compared with single-phase HST. However, when the mass loading is increased to $M = 0.5$ the aerosols cluster, despite their small inertia, and measurably modify the carrier flow. These aerosols enhance turbulence in the carrier phase, causing an increase of the growth rates of the turbulent kinetic energy (TKE) and dissipation rate among other effects. The opposite behavior emerges when the Stokes number is $St_\eta = 0.19$. These aerosols cause the attenuation of turbulence by reducing the growth rates of the TKE and dissipation rate in HST. This attenuation is weaker for the larger mass loading case $M = 0.5$ due to stronger forcing by the particles on the gas in the gravity direction. Turbulence modulation in the EE simulation is verified to hold excellent agreement with EL simulations. In the former approach, simulating a few integral lengths of turbulence leads to a large number of Lagrangian particles, up to 1.7×10^9 particles in the present work. Eulerian-Eulerian simulations are performed with a positivity-preserving kinetic-based formulation that assumes an anisotropic-Maxwellian distribution of the subgrid particle velocity probability distribution function. The excellent agreement with EL simulations shows that this EE simulation strategy is a robust and predictive method in the semidilute regime.

I. INTRODUCTION

Many environmental and technological flows involve dispersed particles or droplets at concentrations large enough to modulate the carrier flow. In the two-way coupling regime, the structure of particle-laden turbulence can differ significantly from its single-phase counterpart [1–7]. The coupling between the two phases renders the derivation of particle-laden turbulence models a challenging task [8]. Understanding how this modulation takes place in canonical flows will help define and validate two-phase models.

---

*houssem.kasbaoui@asu.edu

In the study of turbulence, homogeneously sheared turbulence (HST) is a fundamental flow and a unit block in many turbulence models [9–11]. The flow, in which turbulence is driven by a mean linear shear, is a step up in complexity from the classical homogeneously isotropic turbulence (HIT) and one of the simplest flows that have a generation mechanism of turbulence. It was previously demonstrated that this flow reproduces many of the features of turbulent boundary layers without the added complexity of bounding walls, such as the presence of off-diagonal Reynolds stresses, the generation of hairpin vortices [12–14], and the sweep and ejection mechanisms [15,16]. When inertial aerosols are dispersed in HST, the mean shear may lead to much stronger clustering than would be the case in homogeneous isotropic turbulence, resulting in stronger flow modulation [17]. This is due to the fact that shear is the precursor of the route to clustering [18], a cascade of instabilities in the semidilute regime triggered by shear and one that results in significant clustering. Hence, settling inertial aerosols are expected to cause significant anisotropic forcing on the carrier flow that can lead to a different turbulence structure than in a single-phase flow.

Turbulence modulation by the dispersed phase is complex and remains to be fully understood. In turbulent channel and pipe flows where additives are used to increase the flow throughput by reducing skin-friction drag [19], inertial particles may either increase it [20], decrease it [21,22], or have no significant effect [19,23]. The type of modulation obtained depends on the mass loading M and Stokes number $St_\eta = \tau_p/\tau_\eta$, where τ_p is the particle response time and τ_η is the Kolmogorov timescale. The studies of Tanaka and Teramoto [13] and Ferrante and Elghobashi [24] show that particles with $St_\eta > 1$ reduce the turbulence intensity by reducing the growth rate of the turbulent kinetic energy (TKE) in HST and increasing its decay rate in HIT. However, very small particles having $St_\eta < 0.1$ and massive particles larger than the integral length scale may increase the TKE [24,25]. In the present work, both regimes of turbulence enhancement and attenuation are obtained within the range $St_\eta = 0.06$–0.19 and $M = 0.125$–0.5 in high-shear-number HST.

Part of the challenges in addressing turbulence modulation by inertial particles is the limitation of numerical tools. Current simulation approaches include Eulerian-Lagrangian (EL) and Eulerian-Eulerian (EE) methods. In the former approach, individual particles are tracked and their effect on the gas is accounted for individually. In the semidilute regime, characterized by a volume fraction $\langle \phi \rangle$ in the range 10^{-5}–10^{-3} and an order-one mass loading M, the relatively high particle volume fraction is such that simulating a few integral lengths of a turbulent flow may result in an excessively large number of particles. For this reason, the EL method has been primarily used in particle-laden turbulent flows where the particle concentration is very dilute and the particle feedback on the carrier flow is negligible, i.e., in the one-way coupling regime [26]. Eulerian-Eulerian simulations have the potential to scale better and cost less computationally than EL simulations, but it remains to be shown that they yield correct physics in the semidilute regime, where the multivaluedness of the particle velocity field [27] invalidates classical approaches such as two-fluid methods [18,28]. Recently, a new approach based on kinetic theory was developed [18,29,30] to extend Eulerian methods to the semidilute regime. The method relies on the assumption that the local particle velocity distribution follows an anisotropic-Maxwellian function [31,32]. Kasbaoui *et al.* [18] showed that this approach reproduces all key features of the route to clustering, including the multivaluedness of the particle velocity field. In the present paper, this EE strategy is employed to simulate particle-laden HST and compared with EL simulations.

The present study has two scopes. The first one is to characterize the effect of semidilute inertial aerosols on the carrier gas in strongly sheared HST, with an initial Taylor microscale Reynolds number $Re_{\lambda,0} = 29$ and high shear number $S^* = 27$. The second scope of this study is the verification of a kinetic-based Eulerian-Eulerian simulation strategy against Eulerian-Lagrangian strategy.

The paper is organized as follows. Governing equations and numerical strategies are presented in Secs. II and III, respectively. The simulation setup and parameters are introduced in Sec. IV. To help understand the role of particles in the modification of the carrier turbulence, a discussion of single-phase flow HST is presented in Sec. V. Simulations of HST with particles are then analyzed,

with results pertaining to the gas phase presented in Sec. VI and those pertaining to the dispersed phase presented in Sec. VII. A summary is given in Sec. VIII.

II. GOVERNING EQUATIONS

Consider an incompressible Newtonian gas of density ρ_g and viscosity μ_g loaded with monodisperse solid particles (or liquid droplets) of density ρ_p and diameter d_p at the average volume fraction $\langle\phi\rangle$. In the semidilute regime, the carrier gas satisfies the Navier-Stokes equations

$$\nabla \cdot \mathbf{u}_g = 0, \tag{1}$$

$$\rho_g \frac{\partial \mathbf{u}_g}{\partial t} + \rho_g \mathbf{u}_g \cdot \nabla \mathbf{u}_g = -\nabla p + \mu_g \nabla^2 \mathbf{u}_g + \rho_g \mathbf{g} + \mathbf{F}, \tag{2}$$

where $\mathbf{u}_g$ is the gas velocity, p is the pressure, $\mathbf{g}$ is the gravitational acceleration, and $\mathbf{F}$ represents the momentum exchange between the two phases.

For a discrete particle i, the equations of motion given by Maxey and Riley [33] read

$$\frac{d\mathbf{x}_p^i}{dt} = \mathbf{u}_p^i, \tag{3}$$

$$\frac{d\mathbf{u}_p^i}{dt} = \frac{\mathbf{u}_g(\mathbf{x}_p^i, t) - \mathbf{u}_p^i}{\tau_p} + \mathbf{g}, \tag{4}$$

where $\mathbf{x}_p^i$ and $\mathbf{u}_p^i$ are the Lagrangian position and velocity of the particle and $\tau_p = \rho_p d_p^2 / 18\mu_g$ is the particle response time. Equations (3) and (4) state that the suspended particles experience a hydrodynamic force equal to the Stokes drag and the gravitational force. Other hydrodynamic forces are neglected due to the large density ratio between solid (or liquid) particles and gas. Particle-particle interactions such as collisions, aggregation, and coalescence are also negligible in the regime considered.

The hydrodynamic forces applied on a particle lead to the interphase exchange term

$$\mathbf{F} = \rho_p \phi \frac{\mathbf{u}_p - \mathbf{u}_g}{\tau_p}, \tag{5}$$

where $\mathbf{u}_p$ is the Eulerian particle velocity field and ϕ the local volume fraction. In the Eulerian-Lagrangian formalism, these quantities are determined *a posteriori* from the positions and velocities of individual particles tracked using the equations of motion (3) and (4).

In the Eulerian-Eulerian formalism considered here, the dispersed phase is described with a set of conservation equations derived from kinetic theory of gases [34–40]. Within this formalism, the particle velocity distribution f is subject to a Boltzmann equation in phase space

$$\frac{\partial nf}{\partial t} + \nabla_x \cdot (\mathbf{c}nf) + \nabla_c \cdot \left[\left(\frac{\mathbf{u}_g - \mathbf{c}}{\tau_p} + g \right) nf \right] = 0, \tag{6}$$

where n represents the particle number density. Computationally, it is often more advantageous to consider transport equations for moments of f [41]. The first three moments yield conservation equations for the dispersed phase mass, momentum, and energy

$$\frac{\partial \rho_p n}{\partial t} + \nabla \cdot (\rho_p n \mathbf{u}_p) = 0, \tag{7}$$

$$\frac{\partial (\rho_p n \mathbf{u}_p)}{\partial t} + \nabla \cdot (\mathbf{E}) = \rho_p n \mathbf{g} + \frac{\rho_p n \mathbf{u}_g - (\rho_p n \mathbf{u}_p)}{\tau_p}, \tag{8}$$

$$\frac{\partial \mathbf{E}}{\partial t} + \nabla \cdot (\mathbf{Q}) = \mathbf{g}(\rho_p n \mathbf{u}_p) + (\rho_p n \mathbf{u}_p)\mathbf{g} + \frac{(\rho_p n \mathbf{u}_p)\mathbf{u}_g + \mathbf{u}_g(\rho_p n \mathbf{u}_p) - 2\mathbf{E}}{\tau_p}, \tag{9}$$
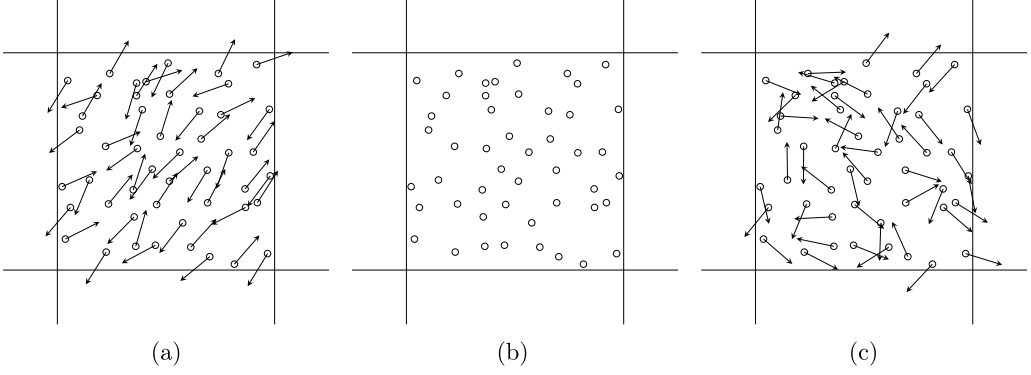
FIG. 1. Illustration of the subgrid particle velocities with the anisotropic-Maxwellian distribution as closure. Arrows represent the particle fluctuating velocity $\mathbf{c} - \mathbf{u}_p$, where $\mathbf{c}$ is the particle velocity and $\mathbf{u}_p$ is the cell averaged velocity. (a) In general, the anisotropic-Maxwellian distribution allows particle-trajectory crossing ($\mathbf{P}_p \neq 0$). (b) In regions of the flow where the particle pressure $\mathbf{P}_p$ vanishes, the velocity fluctuations vanish ($\mathbf{P}_p \to 0$) and the anisotropic-Maxwellian collapses onto the monokinetic distribution. (c) In regions where $\mathbf{P}_p$ becomes isotropic, the anisotropic-Maxwellian collapses onto a Maxwellian distribution ($\mathbf{P}_p \to \Theta \delta_{ij}$).

where $\rho_p \mathbf{u}_p = \int \rho_p n f d\mathbf{c}$, $\mathbf{E} = \int \rho_p n \mathbf{cc} f d\mathbf{c}$, and $\mathbf{Q} = \int \rho_p n \mathbf{ccc} f d\mathbf{c}$ represent the average (local) particle momentum, energy tensor (second order), and heat flux tensor (third order). In this formulation, the coupling term (5) can be readily built from the Eulerian velocity $\mathbf{u}_p$ obtained by solving the particle momentum equation (8) and the local particle volume fraction determined from the local number density solution to Eq. (7).

The conservation equations for the moments of f require closure of the heat-flux term. This can be done by modeling the distribution itself. An appropriate model for semidilute suspensions is given by the anisotropic-Maxwellian (or anisotropic Gaussian) distribution

$$f(\mathbf{c}) = \frac{1}{[2\pi \det(\mathbf{P}_p)]^{2/3}} \exp\left(-\frac{1}{2}(\mathbf{c} - \mathbf{u}_p) \cdot \mathbf{P}_p^{-1}(\mathbf{c} - \mathbf{u}_p) \right), \tag{10}$$

where $\mathbf{P}_p = (\mathbf{E}/\rho_p - \mathbf{u}_p\mathbf{u}_p)/n$ represents the particle pressure tensor. Note that the anisotropic-Maxwellian distribution is a versatile one. When the particle pressure tensor becomes isotropic $\mathbf{P}_p = \Theta \delta_{ij}$, Θ being the particle granular temperature, the distribution f in Eq. (10) collapses onto the Maxwellian distribution $f \to (2\pi\Theta)^{-3/2} \exp[-(\mathbf{c} - \mathbf{u}_p)^2/2\Theta]$, which holds for dense particle-laden flows [37]. When the particle pressure tensors vanishes $\mathbf{P}_p = 0$, the distribution (10) collapses onto a monokinetic distribution $f \to \delta(\mathbf{c} - \mathbf{u}_p)$. This is true for very dilute suspensions [18] and the set of conservation equations for the first three moments become the two-fluid model [3]. These behaviors are illustrated in Fig. 1. The anisotropic-Maxwellian distribution has the property of maximizing entropy given the first three moments [31,32]. Based on recent progress [18,29–32,42], there is growing evidence that closure with the anisotropic-Maxwellian distribution may be an appropriate model of the particle velocity distribution across the full range of dilute to dense suspensions.

It should be noted that other closures have been formulated. Koch [34] closed the equations with a Grad moment expansion about the Maxwellian distribution. Various models based on a quadrature method of moments have been proposed [27,28,41,43–46]. Other closures were based on algebraic relationships between the low-order moments, which are similar in principle to Reynolds-averaged Navier-Stokes modeling but may yield unphysical moments [47,48].

In the present work, turbulence is driven by a mean homogeneous shear flow such that the total velocity is $\mathbf{u}_q = \Gamma x_2 \mathbf{e}_1 + \mathbf{u}'_q$, where Γ is the shear rate, $\mathbf{u}'_q$ is the fluctuating velocity, and $q = p$ or g
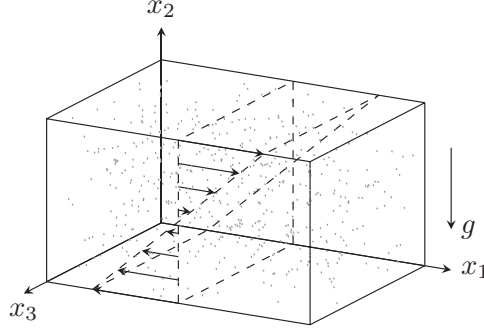
FIG. 2. Sketch of the geometrical configuration. A background base shear $\Gamma x_2 \mathbf{e}_1$ drives a turbulent gas loaded with particles. Gravitational acceleration aligned with the shear direction, i.e., $\mathbf{g} = -g\mathbf{e}_2$, causes the particles to settle.

represents either the particulate or gas phase. A sketch of the configuration is shown in Fig. 2. Note that gravity is parallel to the shear direction x_2 and causes particles to settle. Introducing the velocity decomposition into base shear and fluctuations in the governing equations leads to the emergence of shear distortion terms $[\Gamma x_2 \partial(\cdot)/\partial x_1]$ and bulk shear forcing terms (remaining terms proportional to Γ) [18,49]. For the gas phase, the Navier-Stokes equations expressed for the fluctuations read

$$\nabla \cdot \mathbf{u}'_g = 0, \tag{11}$$

$$\rho_g \frac{\partial \mathbf{u}'_g}{\partial t} + \rho_g \mathbf{u}'_g \cdot \nabla \mathbf{u}'_g = -\nabla p + \mu_g \nabla^2 \mathbf{u}'_g + \rho_g \mathbf{g} + \mathbf{F} - \Gamma x_2 \frac{\partial \mathbf{u}'_g}{\partial x_1} - \Gamma u'_{g,2} \mathbf{e}_1. \tag{12}$$

Similarly, the shear decomposition is introduced in the dispersed phase Eulerian equations

$$\frac{\partial \rho_p n}{\partial t} + \nabla \cdot (\rho_p n \mathbf{u}'_p) = 0 = -\Gamma x_2 \frac{\partial \rho_p n}{\partial x_1}, \tag{13}$$

$$\frac{\partial (\rho_p n \mathbf{u}'_p)}{\partial t} + \nabla \cdot \mathbf{E}' = \rho_p n \mathbf{g} + \frac{\rho_p n \mathbf{u}'_g - \rho_p n \mathbf{u}'_p}{\tau_p} - \Gamma x_2 \frac{\partial \rho_p n \mathbf{u}'_p}{\partial x_1} - \Gamma \rho_p n u'_{p,2} \mathbf{e}_1, \tag{14}$$

$$\frac{\partial \mathbf{E}'}{\partial t} + \nabla \cdot \mathbf{Q} = \mathbf{g}(\rho_p n \mathbf{u}'_p) + (\rho_p n \mathbf{u}'_p)\mathbf{g} \frac{(\rho_p n \mathbf{u}'_p)\mathbf{u}'_g + \mathbf{u}'_g(\rho_p n \mathbf{u}'_p) - 2\mathbf{E}'}{\tau_p}$$

$$-\Gamma x_2 \frac{\partial \mathbf{E}'}{\partial x_1} - \Gamma(\mathbf{E}' \cdot \mathbf{e}_2)\mathbf{e}_1 - \Gamma(\mathbf{E}' \cdot \mathbf{e}_1)\mathbf{e}_2. \tag{15}$$

In the remaining of this paper, the superscript denoting deviation from the base shear will be dropped.

To maintain a true unbounded homogeneous shear, shear-periodic boundary conditions are used in the shear direction x_2 [49] and regular periodicity is used in the streamwise and spanwise directions x_1 and x_3, respectively. For a simulation box that extends from $x_2 = 0$ to L_2 in the shear direction, shear periodicity applied to an Eulerian quantity q requires

$$q(x_1, x_2 = L_2, x_3) = q(x_1 - \Gamma t L_2, x_2 = 0, x_3). \tag{16}$$

The Lagrangian equivalent is the well-known Lees-Edwards conditions and applies to Lagrangian particles.

TABLE I. Simulation parameters for the four cases of particle-laden HST considered.

Parameter	d50L	d50H	d90L	d90H
d_p (μm)	50	50	90	90
ρ_p (kg/m^3)	1200	1200	1200	1200
ρ_f (kg/m^3)	1.2	1.2	1.2	1.2
μ_f (kg/ms)	1.8×10^{-5}	1.8×10^{-5}	1.8×10^{-5}	1.8×10^{-5}
$\langle \phi \rangle$	1.25×10^{-4}	5.0×10^{-4}	1.25×10^{-4}	5.0×10^{-4}
M	0.125	0.5	0.125	0.5
St_η	0.06	0.06	0.19	0.19
St_Γ	0.09	0.09	0.21	0.21
$\tau_p g / u_\eta$	9.4	9.4	30.4	30.4
$Re_{\lambda,0}$	29	29	29	29
S_0^*	27	27	27	27
$L_1 / \Gamma^{-1} \tau_p g$	68.0	68.0	41.6	41.6
$L_2 / \Gamma^{-1} \tau_p g$	34.0	34.0	20.8	20.8
$L_3 / \Gamma^{-1} \tau_p g$	34.0	34.0	20.8	20.8
n_1	512	512	512	512
n_2	256	256	256	256
n_3	256	256	256	256
N	0.327×10^9	1.308×10^9	0.438×10^9	1.752×10^9

III. NUMERICAL METHODS

The simulations are performed with the finite-volume flow solver NGA [50]. The Navier-Stokes equations are discretized with fully conservative second-order schemes on a staggered mesh. The shear forcing terms and shear-periodic boundary conditions are implemented in physical space with a stable mass-, momentum-, and energy-conserving algorithm. Further details of the implementation can be found in Ref. [49].

In Eulerian-Lagrangian simulations, the particle solver follows the method described by Capecelatro and Desjardins [51]. The Lagrangian equations for particle position and velocity are advanced using a second-order Runge-Kutta scheme. The method of Ireland and Desjardins [52] is used to find the unperturbed gas velocity at the particle location. The particle volume fraction is computed from Lagrangian data using a Gaussian filter of width equal to the mesh spacing. Particles that exit the domain in the x_2 direction are reintroduced at a shifted position on the opposite side in accordance with the Lees-Edwards boundary conditions.

In Eulerian-Eulerian simulations, Eqs. (13)–(15) are discretized on a collocated mesh with second-order spatial schemes. Time advancement is performed with a third-order strong-stability-preserving Runge-Kutta scheme. The particle-conservation equations are closed by assuming that the particle velocity distribution is an anisotropic-Maxwellian one [31,32,42,53]. The latter is built with a quadrature method [29,31] using information from the first three moments (number density, mean velocity, and energy tensor). It is then used to close the heat flux term. Overall, the schemes have the realizability property, which ensures the stability of the solver when clustering is significant. This approach captures particle-trajectory crossing effects [18]. The distortion by mean shear is treated in the same manner as in Ref. [49].

IV. RUNS

A series of simulations that explore the role of particle size and mass loading in the modulation of sheared turbulence in the semidilute regime were conducted, and a discussion of the results will now be presented. A summary of the simulation parameters is given in Table I. The carrier gas is air at standard temperature and pressure conditions. The particles considered in this work
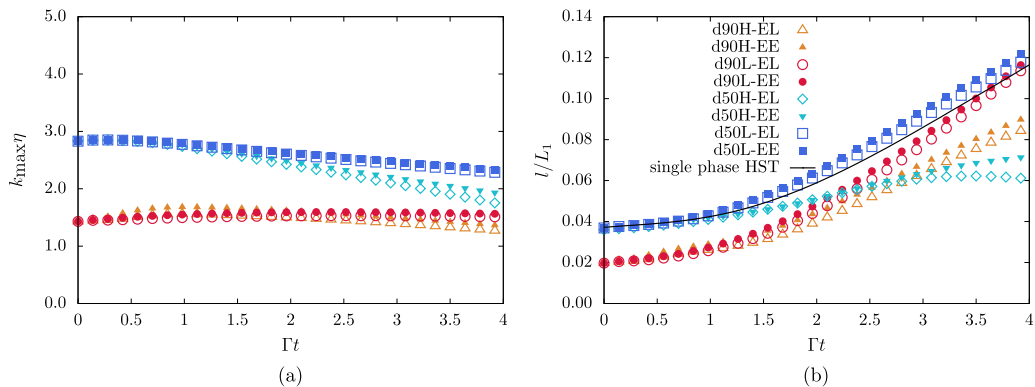
FIG. 3. Evolution of (a) the product of the largest wave number resolved by the grid and the Kolmogorov scale and (b) the normalized integral length scale during the integration time $\Gamma t \leqslant 4$.

have a density $\rho_p = 1200$ kg m^{-3} and a diameter $d_p = 50$ or 90 μm. The average volume fraction $\langle \phi \rangle$ is varied from 1.25×10^{-4} to 5×10^{-4}, which results in a number of Lagrangian particles N between 327×10^6 and 1.7×10^9. The turbulent Stokes number varies between $\mathrm{St}_\eta = \tau_p/\tau_\eta = 0.06$–$0.19$, where τ_η is the Kolmogorov timescale at the beginning of the simulation. The shear Stokes number $\mathrm{St}_\Gamma = \Gamma \tau_p$ varies from 0.09 to 0.021 and is such that the inertial response of particles to shear is as large as their response to turbulent fluctuations ($\mathrm{St}_\Gamma \sim \mathrm{St}_\eta$). The mass loading varies from $M = 0.125$ to 0.5. At these values, the two-way coupling is significant, although it may be weak for $M = 0.125$. All simulations were performed with the EL and EE approaches. Turbulence modulation is assessed by comparison with additional simulations of HST without particles, i.e., single-phase flow turbulence.

In all cases considered, the initial turbulence in the carrier gas is unchanged. The initial Taylor microscale Reynolds number is $\mathrm{Re}_{\lambda,0} = 29$. The flow is sheared at the constant rate $\Gamma = 7$ s^{-1}, yielding a shear number $S_0^* = 2\Gamma k_0/\epsilon_0 = 27$, where k_0 and ϵ_0 are the turbulent kinetic energy and dissipation rate at $t = 0$, respectively. Note that at such high shear number, the early evolution of turbulence will be strongly impacted by the shear distortion. The evolution of the sheared particle-laden flow is considered until a total deformation $\Gamma t = 4$.

The resolution selected for the present simulations is driven by the need to strike a compromise between (a) resolving the smallest scales of the flow, (b) having coarse enough cells to encompass a sufficient number of Lagrangian particles for proper statistical sampling, (c) having a large enough computational box that allows the unconstrained elongation of vortical structures and particle clusters, and (d) having a small enough computational box such that the number of Lagrangian particles remains trackable. A good compromise can be achieved with a uniform grid of size $512 \times 256 \times 256$ and the box sizes listed in Table I. In all cases selected, the grid resolution ensures that the smallest features of the flow are captured as shown by $k_{\max}\eta \geqslant 1$ in Fig. 3(a), where $k_{\max}$ is the largest wave number supported by the grid. With the given computational box dimensions, the large scales of the flow are also resolved as evidenced by the small ratio of the integral length scale $l \equiv \langle u_1^2 \rangle^{3/2}/\epsilon$ [54] to the longitudinal dimension L_1 shown in Fig. 3(b). Additionally, by maintaining $L_2/L_g > 20$, where $L_g \equiv \Gamma^{-1}\tau_p g$ is the characteristic particle settling distance in homogeneous shear [55], one ensures enough space in the computational domain to allow the elongation of particle clusters by gravity. In Eulerian-Lagrangian simulations, the resolution thus selected yields an average number of particles per cell between 9.7 for case d50L and 52.2 for case d90H. Although among the largest to date, the total count of Lagrangian particles remains trackable. Further information on the grid convergence properties of the particle-phase solvers is provided in Ref. [30].
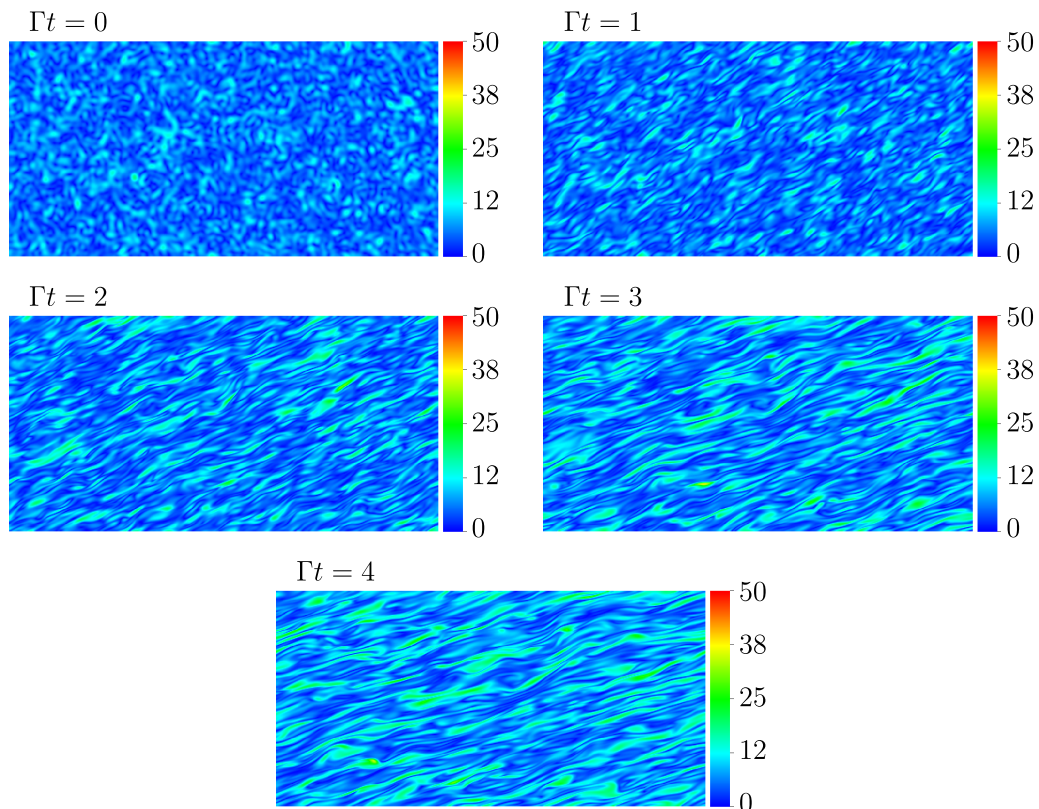
FIG. 4. Snapshots of isocontours of vorticity magnitude in the x_1-x_2 plane at $\Gamma t = 4$ from a single-phase flow simulation of homogeneously sheared turbulence.

V. SINGLE-PHASE HST

The reference flow of this study is single-phase HST. In this section, the evolution of turbulence will be discussed qualitatively. Thorough quantitative analyses have been discussed in previous studies [49].

Figure 4 shows isocontours of vorticity magnitude from $\Gamma t = 0$ to $\Gamma t = 4$. Initially, the flow is isotropic and periodic in all directions. As time progresses, a strongly anisotropic flow develops characterized by long vortical structures oriented in the streamwise direction. The imposed linear shear stretches vortical tubes and sheets and causes them to become nearly parallel to the x_1 direction. The linear shear also causes the compression of vortex sheets in the shear direction x_2. It is noteworthy that the vorticity magnitude increases over time in Fig. 4. This is due to the energy injection by mean shear, which causes the turbulent kinetic energy and dissipation rate to grow at an exponential rate for large-shear-number flows [49,56,57].

The early-stage evolution of the flow (up until $\Gamma t \sim 1$) can be described by rapid distortion theory [49,58–61]. During this phase, the shear distortion terms vastly exceed the nonlinear inertial terms. As such, the flow is amenable to analytical treatment and it can be shown that the turbulence evolution is solely controlled by the shearing motion.

Rapid distortion ends when the compression of vortical sheets becomes so large that the nonlinear inertial terms become significant. At large times ($\Gamma t > 20$), a balance is established between the nonlinearities and distortion leading to a universal self-similar state [49,54,62–65]. In the case of particle-laden HST, it may be expected that the dispersed phase will break the self-similar behavior
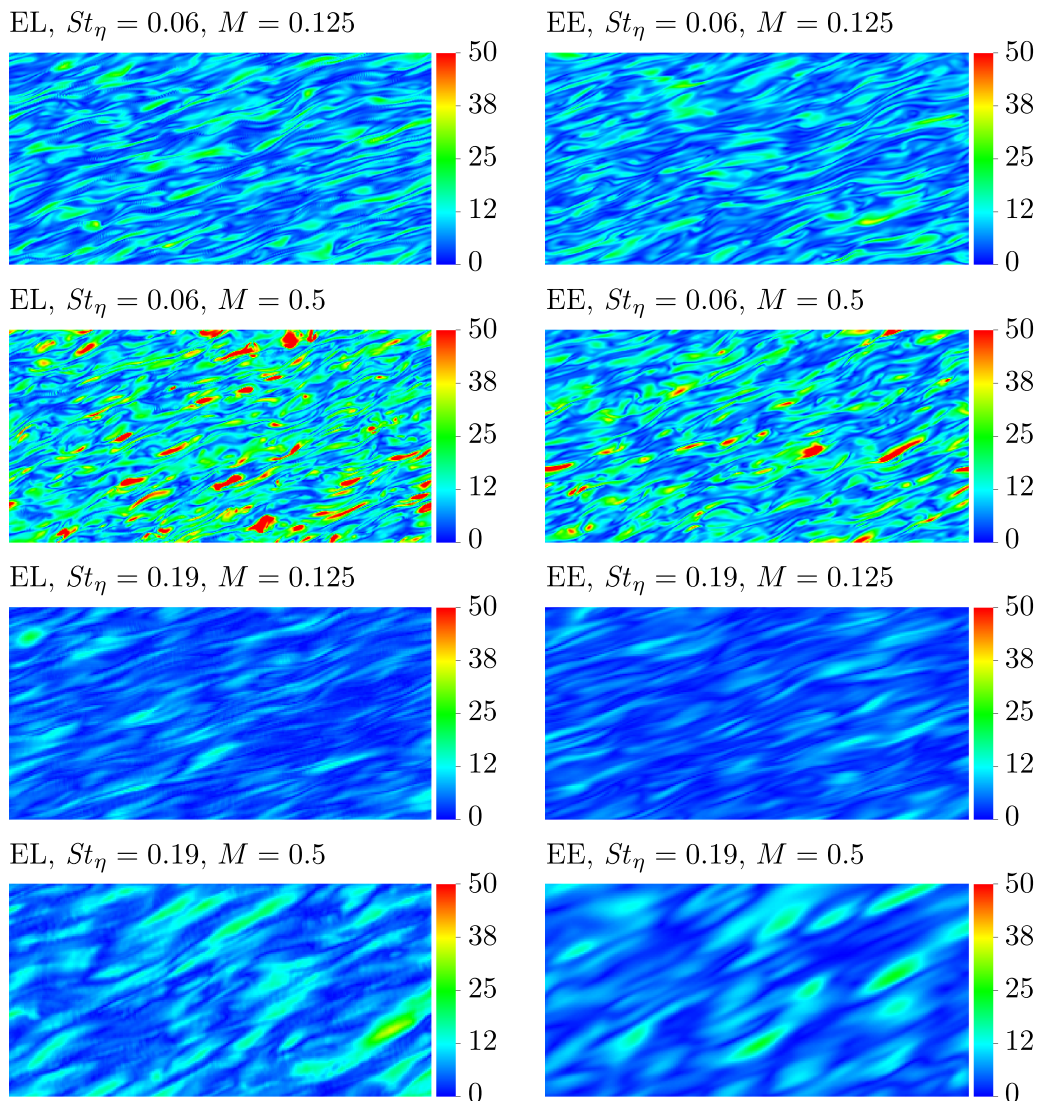
FIG. 5. Isocontours of vorticity magnitude in the x_1-x_2 plane at $\Gamma t = 4$ from EL and EE simulations in Table I.

as it introduces new timescales and length scales [17]. In the present work, we stop the simulations at $\Gamma t = 4$, after the rapid distortion ends and well before the establishment of a self-similar regime.

VI. TURBULENCE MODULATION

The addition of settling particles to the gas leads to an evolution of particle-laden HST that may be different from the evolution in the single-phase flow case. The coupling between the two phases can change the structure of turbulence in the carrier gas. The degree to which turbulence is modulated depends on the Stokes number St_η and mass loading M. The effects of these two quantities are investigated in the following. For the four two-phase flow cases considered, snapshots of the vorticity magnitude at $\Gamma t = 4$ are shown in Fig. 5. Images from the Eulerian-Lagrangian and Eulerian-Eulerian simulations are shown side by side to facilitate visual comparison. Comparing

with the single-phase flow in Fig. 4, it is clear that the presence of particles leads to a varying degree of modification of the vortical structures. Qualitatively, case d50L ($St_\eta = 0.06$ and $M = 0.125$) displays the most similarity with the single-phase flow case, while case d90H ($St_\eta = 0.19$ and $M = 0.125$) displays the largest modulation of the turbulence structure. The nature of the turbulence modulation depends on the mass loading and Stokes number. These will be discussed in further detail in Secs. VI A–VI D.

Before going further, it is worthwhile to address a point regarding results obtained with Eulerian-Eulerian and Eulerian-Lagrangian methods. It was found that the two simulation methods predict a similar amount of turbulence modulation by the dispersed phase. This may be seen from the isocontours of vorticity magnitude that appear substantially similar regardless of the method used. The analysis of turbulence modulation by the particle phase lends itself to the same conclusions about the physics of the flow regardless of the particle-phase framework considered. Hence, when discussing statistics of the carrier phase in Secs. VI A–VI D, no distinction will be made between Eulerian-Eulerian or Eulerian-Lagrangian simulations. The quantitative differences from the two methods will be addressed in Sec. VI E.

A. Small Stokes number and small mass loading

Consider the case of $d_p = 50$ μm particles dispersed in air at $\langle \phi \rangle = 1.25 \times 10^{-4}$ (run d50L in Table I). In this flow, the mass loading is $M = 0.125$ and the Stokes number is $St_\eta = 0.06$.

Here the dispersed phase has no significant effect on the carrier turbulence. The isocontours of vorticity magnitude in Fig. 5 show little difference with the particle-free case in Fig. 4. Turbulence statistics shown in Fig. 6 depict an evolution of particle-laden HST that closely follows the evolution of single-phase HST. The growth rates of the dissipation rate ϵ and TKE k remain unchanged [see Figs. 6(a) and 6(b)], suggesting that the two-way coupling effects are negligible and that the turbulence evolution is controlled primarily by the linear shear. This is further confirmed by the shear production term $\mathcal{P} = -\Gamma \langle u_1 u_2 \rangle$ in Fig. 6(c), which evolves similarly to single-phase HST.

The stretching of vortical structures in the streamwise direction can be quantified using the streamwise Taylor microscale λ_{11}. Aerosols in the case d50L do not lead to any more or less stretching of the vortical structures in the x_1 direction, as evidenced by the nearly identical evolution of λ_{11} [see Fig. 6(d)] in the one-phase and two-phase cases. Additionally, none of the diagonal components of the anisotropic Reynolds stresses $b_{ij} = \langle u_i u_j \rangle / \langle u_i u_i \rangle - \delta_{ij}/3$ shown in Fig. 7(a) are altered by the inertial aerosols.

The absence of turbulence modulation in this case is expected due to the small values of Stokes number and mass loading ($St_\eta = 0.06$ and $M = 0.125$). Due to their small inertia, the particles tend to mostly follow the gas path lines. It should be noted that, despite the small value of St_η, these particles should not be considered as tracer particles since the presence of a persistent mean shear motion may still lead to non-negligible preferential concentration effects. In this case, the mass loading $M = 0.125$ is too small for any significant interphase coupling effects to manifest by $\Gamma t = 4$.

B. Small Stokes number and moderate mass loading

In the case d50H, the dispersed phase is characterized by the pair of nondimensional numbers ($St_\eta = 0.06$ and $M = 0.5$). The higher mass loading is achieved by an increase of the volume fraction to $\langle \phi \rangle = 5 \times 10^{-4}$, thus leaving the Stokes number identical to the previous case.

With higher mass loading ($M = 0.5$), turbulence modulation becomes significant. Figure 5 shows a modification of the flow structures, wherein the gas flow vorticity attains a higher magnitude at $\Gamma t = 4$ compared with the single-phase flow case in Fig. 4. The strengthening of vorticity indicates an enhancement of turbulence in this case. There is also evidence of a modulation of the flow anisotropy since the vortical structures appear less elongated in the presence of particles.
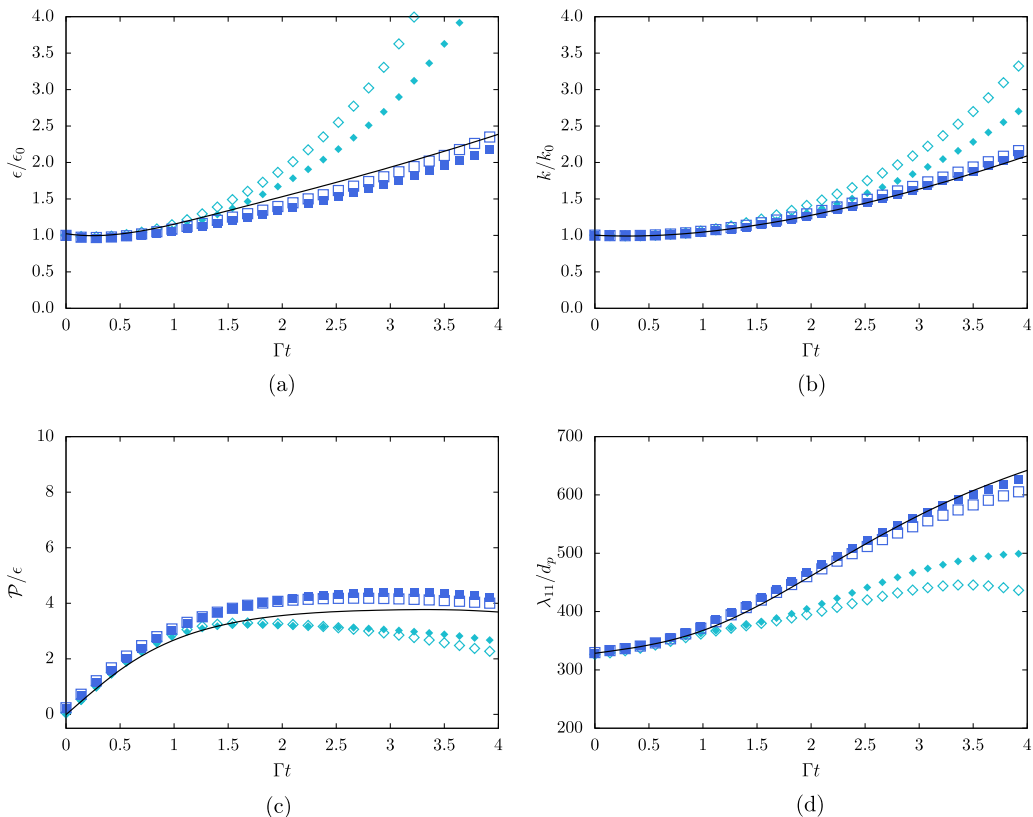
FIG. 6. Turbulence statistics from EL (open symbols), EE (closed symbols), and single-phase HST (lines) simulations for the two cases with $St_\eta = 0.06$ particles: (a) normalized dissipation rate, (b) normalized turbulent kinetic energy, (c) ratio of shear production to dissipation rates, and (d) normalized streamwise Taylor microscale. Symbols □ and ■ refer to case d50L having a mass loading $M = 0.125$. Symbols ◇ and ◆ refer to case d90H having a mass loading $M = 0.5$.

The dispersed phases enhances turbulence in this case. The TKE k and dissipation rate ϵ shown in Figs. 6(b) and 6(a) grow at a faster rate compared with single-phase HST and case d50L ($St_\eta = 0.06$ and $M = 0.125$). The increase of k is due to the forcing that settling particles exert on the flow [55]. As Elghobashi and Truesdell [4] explain, particles force the flow on a scale comparable to the viscous dissipation scale, thus causing an increase of dissipation rate. Kasbaoui *et al.* [55] show from linear stability analysis that the interplay between shear and preferential concentration leads to a forcing of the flow that occurs primarily on a scale $\sqrt{\nu/\Gamma} = \eta\sqrt{St_\eta/St_\Gamma} \sim \eta$. Fluctuations at the Kolmogorov scale increase the dissipation rate, thus reducing the ratio of shear production $\mathcal{P}$ to ϵ in Fig. 6(c).

The coupling with the dispersed phase changes the structure of anisotropy in the flow. The extent of turbulent structures in the streamwise direction is reduced, as can be seen from the snapshots in Fig. 5 and from the decrease of λ_{11} [see Fig. 6(d)]. This can also be seen from the diminishing anisotropic Reynolds stress component b_{11} in Fig. 7(b). Conversely, the flow anisotropy in the direction of gravity (which is also the shear direction), measured by b_{22}, is increased, a result of the strengthening effects of particle settling on the carrier gas due to the larger mass loading. There is also an extension of turbulent structures in the spanwise direction characterized by an increase in b_{33}. These results show that there is a competition between the anisotropy induced by the shear and the one induced by particle settling.
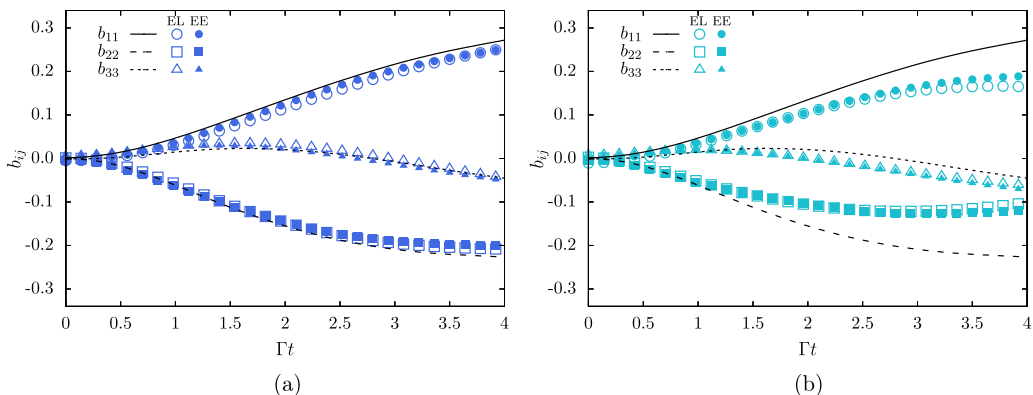
FIG. 7. Diagonal components of the anisotropic Reynolds stress tensor from EL (open symbols), EE (closed symbols), and single-phase HST (lines) simulations for the two cases with $St_\eta = 0.06$ particles: (a) $M = 0.125$ and (b) $M = 0.5$.

C. Moderate Stokes number and small mass loading

In the case d90L, the Stokes number is increased to $St_\eta = 0.19$ by increasing the particle diameter to $d_p = 90$ μm. The particle volume fraction is $\langle\phi\rangle = 1.25 \times 10^{-4}$, resulting in a mass loading $M = 0.125$.

Here the dispersed phase causes an attenuation of turbulence. Evidence of lower turbulence intensity can be immediately seen from the drop of vorticity magnitude in Fig. 5. Note that this modulation is a consequence of the increase of particle inertia, since there was no turbulence modulation for the case d50L with the same mass loading $M = 0.125$ and lower Stokes number $St_\eta = 0.06$. Quantitatively, the turbulence attenuation is a result of the reduced growth rates of TKE and ϵ shown in Figs. 8(b) and 8(a). In single-phase HST, the TKE growth rate is exclusively controlled by the ratio of shear production to dissipation rate. However, here $\mathcal{P}/\epsilon$ increases despite a slowing k [see Fig. 8(c)]. This trend suggests a strengthening of the energy transfer between the two phases and weakening of energy injection by mean shear.

Increasing the Stokes number to $St_\eta = 0.19$ leads to a different effect on the flow anisotropy. In this case, the vortical structures are further elongated in the x_1 direction, resulting in a larger λ_{11}, seen in Fig. 8(d). Compared with single-phase HST, the anisotropic Reynolds stress component b_{22} remains unaffected by the dispersed phase [see Fig. 9(a)]. However, there is an increase in the component b_{11} and a decrease in b_{33}. Hence, the effect of turbulence attenuation is larger in the spanwise direction x_3. Overall, the dispersed phase aids shear in concentrating the carrier flow energy in the streamwise direction.

D. Moderate Stokes number and moderate mass loading

For this final case d90H, the Stokes number is $St_\eta = 0.19$, while the mass loading is increased to $M = 0.5$. Similarly to the previous cases, the increase of mass loading is achieved through an increase of the average volume fraction, thus maintaining the same Stokes number as in d90L ($St_\eta = 0.06$ and $M = 0.125$).

The turbulence modulation in this case is qualitatively similar to the case d90L with lower mass loading. Compared with single-phase HST, there is an attenuation of turbulence characterized by a drop in vorticity magnitude (see Fig. 5) and a reduction in the growth rates of the turbulent kinetic energy and dissipation rate [see Figs. 8(b) and 8(a)]. However, the larger mass loading leads to less turbulence attenuation than in the case d90L. The quantities ϵ and k grow faster at $M = 0.5$ than at $M = 0.125$, due to the strengthening of the energy transfer mechanism from the particulate to gas phase. Note that there is a strong reduction of b_{33} accompanied by a significant increase of
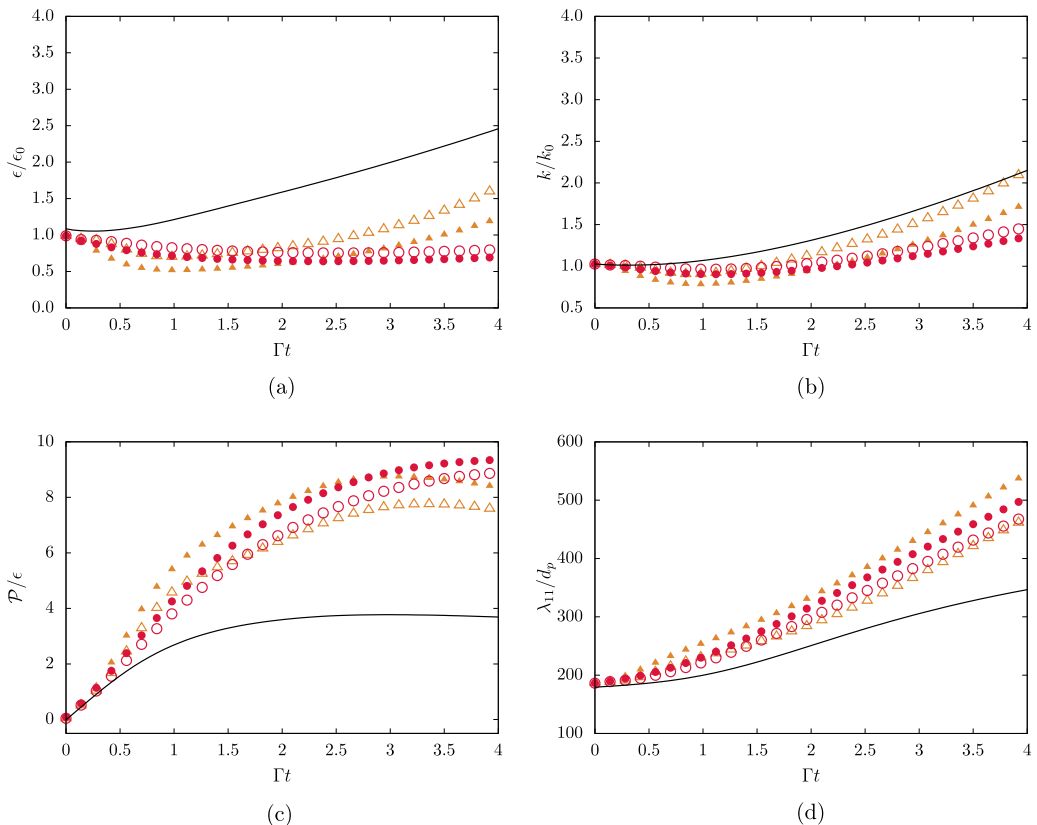
FIG. 8. Turbulence statistics from EL (open symbols), EE (closed symbols), and single-phase HST (lines) simulations for the two cases with $St_\eta = 0.19$ particles: (a) normalized dissipation ratio, (b) normalized turbulent kinetic energy, (c) ratio of shear production to dissipation rates, and (d) normalized streamwise Taylor microscale. Symbols ○ and ● refer to case d90L having a mass loading $M = 0.125$. Symbols △ and ▲ refer to case d90H having a mass loading $M = 0.5$.

b_{22}. This may be due to the formation of particle clusters (see Fig. 10) that exert a stronger forcing on the gas as they settle in the gravitational direction x_2. These clusters damp fluctuations in the spanwise direction where there is no gravity or shear to aid the gas in displacing these heavier particle structures.

E. Differences in the carrier phase statistics between Eulerian-Eulerian and Eulerian-Lagrangian simulations

The statistics of the carrier gas discussed so far show similar turbulence modulation and trends in both Eulerian-Eulerian and Eulerian-Lagrangian methods. Quantitatively, the agreement holds very well for quantities based on the Reynolds stresses $\langle u_i u_j \rangle$, such as TKE, shear production, and anisotropic stresses b_{ij} (see Figs. 8 and 6). Growth of these terms matches well between Eulerian-Eulerian and Eulerian-Lagrangian simulations, since the gas Reynolds-stress tensor components are primarily produced at the integral scale [8] where the two methods perform similarly.

The largest deviation between the two simulation approaches is seen for the dissipation rate. Simulations with the Eulerian-Lagrangian method generally display larger ϵ. As noted by Ahmed and Elghobashi [7], Lagrangian particles create small local velocity gradients that increase the local strain rate, which in turn leads to an increase of the dissipation rate. Various investigators
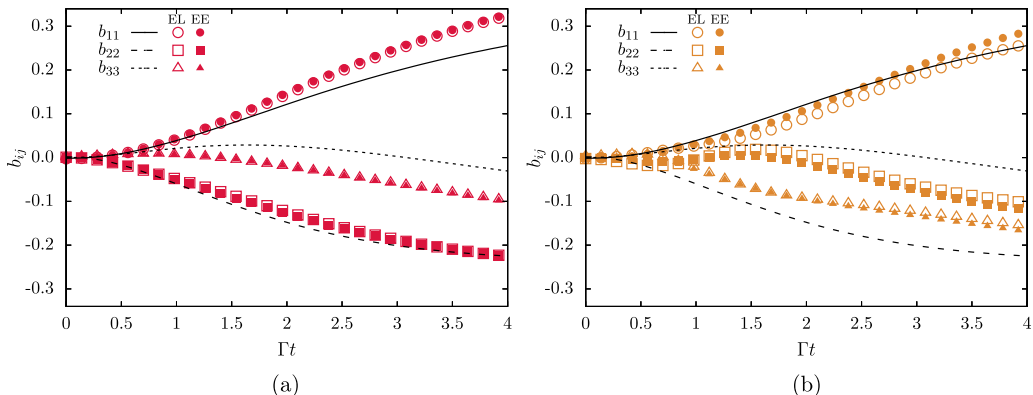
FIG. 9. Diagonal components of the anisotropic Reynolds stress tensor from EL (open symbols), EE (closed symbols), and single-phase HST (lines) simulations for the two cases with $St_\eta = 0.19$ particles: (a) $M = 0.125$ and (b) $M = 0.5$.

[7,66–68] showed that small-Stokes-number Lagrangian particles induce fluctuations at or below the Kolmogorov length scale. Due to resolution limits, fluctuations at these scales cannot be produced in Eulerian-Eulerian simulations, which may explain the lower dissipation rate. However, one needs to acknowledge that the dissipation rate in Eulerian-Lagrangian simulations is subject to uncertainty. As explained by Xu and Subramaniam [69], the accurate approximation of particle drag in Eulerian-Lagrangian methods does not guarantee an accurate gas-phase dissipation rate in the presence of particles. The fact that the two simulation approaches lead to similar trends for the dissipation rate with limited quantitative difference, in all four cases presented, is a satisfactory result.

VII. PARTICLE PHASE

In the semidilute regime, the inhomogeneous particle distribution impacts significantly the forcing exerted on the gas momentum. As it may be seen from the interphase coupling term [Eq. (5)], regions with higher local particle volume fraction ϕ create stronger forcing on the gas compared with regions with lower ϕ. This is in addition to the fact that regions where particles accumulate, i.e., particle clusters, usually have larger slip velocity [6,70,71]. It follows that the turbulence modulation depends strongly on the way inertial aerosols are distributed and cluster in the domain.

Snapshots of the local volume fraction are shown in Fig. 10. By the time $\Gamma t = 4$, the degree of clustering varies sharply between the four cases considered. Case d50L ($St_\eta = 0.06$ and $M = 0.125$) displays only a mildly inhomogeneous particle distribution, likely due to the small Stokes number and weak coupling between the two phases. Despite the similarly low Stokes number in case d50H ($St_\eta = 0.06$ and $M = 0.5$), the larger mass loading causes a strengthening of preferential concentration effects. In this case, particle clusters adjacent to nearly depleted regions can be seen in the Eulerian-Lagrangian simulations and to a lower degree in the Eulerian-Eulerian simulations. These structures are elongated in the streamwise direction, similarly to the way vortical structures are stretched. The regions of highest concentration have a volume fraction that is over twice the average. Previous studies performed in homogeneous isotropic turbulence concluded that particles with very low Stokes number display weak clustering [6,68,72]. Here it is clear that persistent shear amplifies clustering significantly. In cases d90L ($St_\eta = 0.19$ and $M = 0.125$) and d90H ($St_\eta = 0.19$ and $M = 0.5$) the particles are also found to be distributed inhomogeneously. Weak clustering is found for the case with lower mass loading, although the structures appear longer than in the case d50L. The longest clusters are found in case d90H, where these structures are tilted towards the streamwise direction.
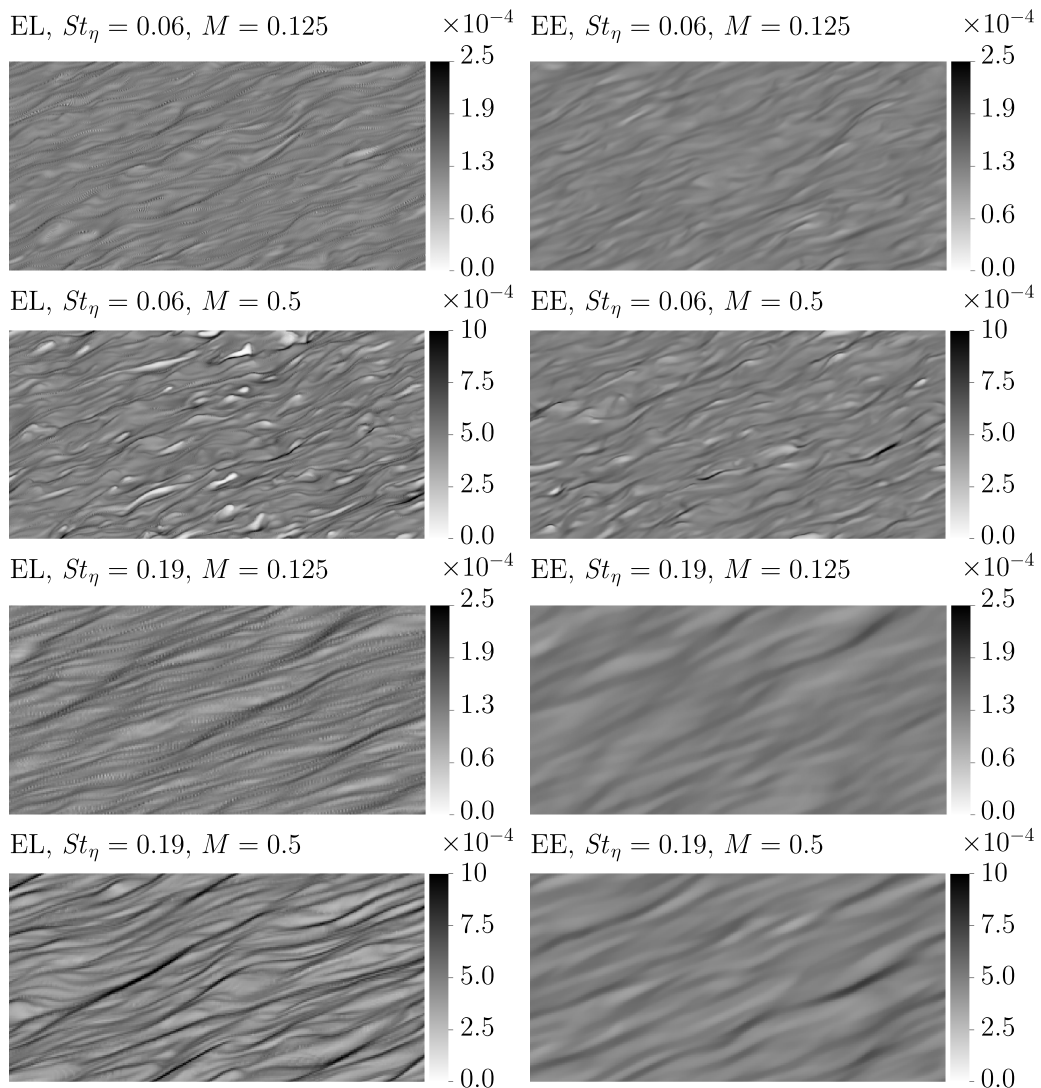
FIG. 10. Isocontours of volume fraction in the x_1-x_2 plane at $\Gamma t = 4$ from EL and EE simulations in Table I.

Figures 11(a) and 11(b) show the evolution of volume fraction fluctuations for the four particle-laden HST simulations. The growth of volume fraction fluctuations reflects the development of in-homogeneities in the particle distribution. Qualitatively, Eulerian-Eulerian and Eulerian-Lagrangian simulations predict similar evolutions, with a quantitative agreement that extends until $\Gamma t \sim 2$ for the cases with $St_\eta = 0.06$ and $\Gamma t \sim 1$ for the cases with $St_\eta = 0.19$. As the simulations approach $\Gamma t = 4$, one can see a large departure between the volume fractions fluctuations predicted by the two simulation strategies.

It is clear that the differences in the rms of particle volume fraction fluctuation between EE and EL simulations do not translate into different turbulence modulation. The anisotropic Reynolds stresses shown in Figs. 7(a), 7(b), 9(a), and 9(b) show excellent agreement between the two simulation strategies. This suggests that the differences in particle volume fraction fluctuations may be related more to differences in the numerical approaches rather than physical processes.
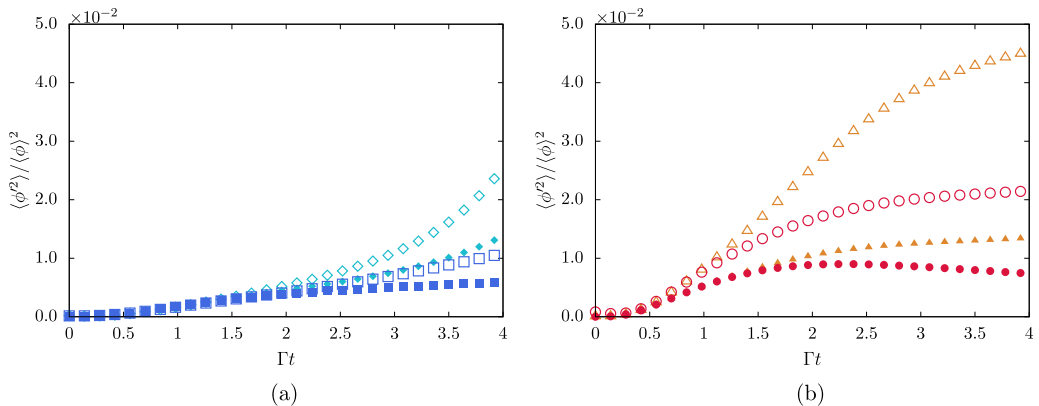
FIG. 11. Volume fraction fluctuations in EL (open symbols) and EE (closed symbols) simulations for (a) $St_\eta = 0.06$ and (b) $St_\eta = 0.19$. Symbols are the same as in Figs. 6 and 8.

Where clustering is strong and the particle structures are thin, a difference between the Eulerian-Eulerian and Eulerian-Lagrangian simulations can be seen. In the former approach, the discrete particles, which are collisionless in this study, may concentrate into arbitrary thin structures. Thus, the volume fraction computed from the particle positions may display very sharp gradients near particle clusters [30]. In the Eulerian-Eulerian simulation strategy, the volume fraction obtained from solving the particle conservation equations is limited by the mesh resolution and the order of accuracy the schemes used, second order in space here. Hence, the volume fraction field obtained this way is unable to display gradients as sharp as those found from Eulerian-Lagrangian simulations.

VIII. CONCLUSION

In the semidilute regime, the forcing exerted by particles on the gas may lead to substantial modification of the suspending turbulence. The analysis of the canonical homogeneously sheared turbulence loaded with inertial aerosols has revealed that the dispersed phase may either enhance or weaken turbulence, depending on the particle Stokes number St_η and mass loading M. The particles also cause a modification of the topology of the vortical structures and a reorganization of the turbulence anisotropy. The present work has illustrated the complexity of flow modification with inertial spherical particles.

The case where $St_\eta = 0.06$ and $M = 0.125$ shows little modification of turbulence, understandably due to the weak particle inertia and coupling between the two phases. However, when the mass loading increases to $M = 0.5$, the suspended particles cluster and lead to a measurable augmentation of turbulence. Particles in this regime inject momentum fluctuations at a scale η [55], which enhances the dissipation rate and turbulent kinetic energy. The persistent linear shear and strong coupling lead to an activation of clustering (route to clustering in Ref. [18]) and formation of void bubbles greater than typically observed in the absence of strong mean shear. Particle settling modifies the anisotropic Reynolds stresses, causing an increase of the component in the direction of gravity.

The introduction of larger particles with $St_\eta = 0.19$ in HST leads to an attenuation of kinetic energy and dissipation rate even for the low mass loading $M = 0.125$. The particles significantly alter the vortical structures, causing them to stretch more in the streamwise direction, which leads to an increase of the streamwise anisotropic Reynolds component. The clusters also appear larger and more elongated in the x_1 direction. Increasing the mass loading $M = 0.5$ reduces the turbulence attention due to stronger clustering and more turbulent fluctuations along the gravity direction.

This paper also addressed the suitability of a recent kinetic-based Eulerian-Eulerian numerical strategy [18,29–32] for simulations of strongly sheared particle-laden flows in the semidilute regime. Comparison with Eulerian-Lagrangian simulations showed similar turbulence modulation trends. Despite some differences in the gas-phase dissipation rate, both methods predicted the modulation of anisotropic Reynolds stresses, with excellent agreement in all four cases considered. However, the rms of particle volume fraction fluctuations was larger in EL simulations, due to the emergence of particle features smaller than the mesh resolution, which cannot be reproduced in EE simulation [30]. These differences do not result in any significant changes in the clustering patterns or flow modulation, hence showing that the EE simulation methodology used here performs excellently in the semidilute regime.

[1] F. Battista, P. Gualtieri, J.-P. Mollicone, and C. Casciola, Application of the exact regularized point particle method (ERPP) to particle laden turbulent shear flows in the two-way coupling regime, Int. J. Multiphase Flow **101**, 113 (2018).

[2] P. Gualtieri, F. Picano, G. Sardina, and C. M. Casciola, Clustering and turbulence modulation in particle-laden shear flows, J. Fluid Mech. **715**, 134 (2013).

[3] O. A. Druzhinin, On the two-way interaction in two-dimensional particle-laden flows: The accumulation of particles and flow modification, J. Fluid Mech. **297**, 49 (1995).

[4] S. Elghobashi and G. C. Truesdell, On the two-way interaction between homogeneous turbulence and dispersed solid particles. I: Turbulence modification, Phys. Fluids A **5**, 1790 (1993).

[5] O. A. Druzhinin, The influence of particle inertia on the two-way coupling and modification of isotropic turbulence by microparticles, Phys. Fluids **13**, 3738 (2001).

[6] T. S. Yang and S. S. Shy, Two-way interaction between solid particles and homogeneous air turbulence: Particle settling rate and turbulence modification measurements, J. Fluid Mech. **526**, 171 (2005).

[7] A. M. Ahmed and S. Elghobashi, On the mechanisms of modifying the structure of turbulent homogeneous shear flows by dispersed particles, Phys. Fluids **12**, 2906 (2000).

[8] R. O. Fox, On multiphase turbulence models for collisional fluid-particle flows, J. Fluid Mech. **742**, 368 (2014).

[9] J. L. Lumley, in *Advances in Applied Mechanics*, edited by C.-S. Yih (Elsevier, Amsterdam, 1979), Vol. 18, pp. 123–176.

[10] A. Briard, T. Gomez, V. Mons, and P. Sagaut, Decay and growth laws in homogeneous shear turbulence, J. Turbul. **17**, 699 (2016).

[11] P. Sagaut and C. Cambon, *Homogeneous Turbulence Dynamics* (Cambridge University Press, New York, 2008).

[12] M. Tanaka and S. Kida, Characterization of vortex tubes and sheets, Phys. Fluids A **5**, 2079 (1993).

[13] M. Tanaka and D. Teramoto, Modulation of homogeneous shear turbulence laden with finite-size particles, J. Turbul. **16**, 979 (2015).

[14] M. Tanaka, Effect of gravity on the development of homogeneous shear turbulence laden with finite-size particles, J. Turbul. **18**, 1144 (2017).

[15] A. Pumir and B. I. Shraiman, Persistent Small Scale Anisotropy in Homogeneous Shear Flows, Phys. Rev. Lett. **75**, 3114 (1995).

[16] A. Pumir, Turbulence in homogeneous shear flows, Phys. Fluids **8**, 3112 (1996).

[17] M. H. Kasbaoui, D. L. Koch, and O. Desjardins, The rapid distortion of two-way coupled particle-laden turbulence, J. Fluid Mech. **877**, 82 (2019).

[18] M. H. Kasbaoui, D. L. Koch, and O. Desjardins, Clustering in Euler-Euler and Euler-Lagrange simulations of unbounded homogeneous particle-laden shear, J. Fluid Mech. **859**, 174 (2019).

[19] A. Gyr and H.-W. Bewersdorff, *Drag Reduction of Turbulent Flows by Additives*, Fluid Mechanics and its Applications Vol. 32 (Springer Netherlands, Dordrecht, 1995).

[20] Y. Li, J. B. McLaughlin, K. Kontomaris, and L. Portela, Numerical simulation of particle-laden turbulent channel flow, Phys. Fluids **13**, 2957 (2001).

[21] X. Shao, T. Wu, and Z. Yu, Fully resolved numerical simulation of particle-laden turbulent flow in a horizontal channel at a low Reynolds number, J. Fluid Mech. **693**, 319 (2012).

[22] L. H. Zhao, H. I. Andersson, and J. J. J. Gillissen, Turbulence modulation and drag reduction by spherical particles, Phys. Fluids **22**, 081702 (2010).

[23] I. Radin, J. L. Zakin, and G. K. Patterson, Drag reduction in solid-fluid systems, AIChE J. **21**, 358 (1975).

[24] A. Ferrante and S. Elghobashi, On the physical mechanisms of two-way coupling in particle-laden isotropic turbulence, Phys. Fluids **15**, 315 (2003).

[25] R. A. Gore and C. T. Crowe, Effect of particle size on modulating turbulent intensity, Int. J. Multiphase Flow **15**, 279 (1989).

[26] J. Ferry and S. Balachandar, A fast Eulerian method for disperse two-phase flow, Int. J. Multiphase Flow **27**, 1199 (2001).

[27] R. O. Fox, Large-eddy-simulation tools for multiphase flows, Annu. Rev. Fluid Mech. **44**, 47 (2012).

[28] O. Desjardins, R. O. Fox, and P. Villedieu, A quadrature-based moment method for dilute fluid-particle flows, J. Comput. Phys. **227**, 2514 (2008).

[29] B. Kong, R. O. Fox, H. Feng, J. Capecelatro, R. Patel, O. Desjardins, and R. O. Fox, Euler-Euler anisotropic gaussian mesoscale simulation of homogeneous cluster-induced gas-particle turbulence, AIChE J. **63**, 2630 (2017).

[30] R. G. Patel, O. Desjardins, B. Kong, J. Capecelatro, and R. O. Fox, Verification of Eulerian-Eulerian and Eulerian-Lagrangian simulations for turbulent fluid–particle flows, AIChE J. **63**, 5396 (2017).

[31] A. Vié, F. Doisneau, and M. Massot, On the anisotropic Gaussian velocity closure for inertial-particle laden flows, Commun. Comput. Phys. **17**, 1 (2015).

[32] S. Saha and M. Alam, Revisiting ignited-quenched transition and the non-Newtonian rheology of a sheared dilute gas-solid suspension, J. Fluid Mech. **833**, 206 (2017).

[33] M. R. Maxey and J. J. Riley, Equation of motion for a small rigid sphere in a nonuniform flow, Phys. Fluids **26**, 883 (1983).

[34] D. L. Koch, Kinetic theory for a monodisperse gas-solid suspension, Phys. Fluids A **2**, 1711 (1990).

[35] M. Y. Louge, E. Mastorakos, and J. T. Jenkins, The role of particle collisions in pneumatic transport, J. Fluid Mech. **231**, 345 (1991).

[36] J.-F. Parmentier and O. Simonin, Transition models from the quenched to ignited states for flows of inertial particles suspended in a simple sheared viscous fluid, J. Fluid Mech. **711**, 147 (2012).

[37] A. S. Sangani, G. Mo, H.-K. Tsao, and D. L. Koch, Simple shear flows of dense gas-solid suspensions at finite Stokes numbers, J. Fluid Mech. **313**, 309 (1996).

[38] H.-K. Tsao and D. L. Koch, Simple shear flows of dilute gas-solid suspensions, J. Fluid Mech. **296**, 211 (1995).

[39] S. Chapman, T. G. Cowling, and D. Burnett, *The Mathematical Theory of Non-Uniform Gases: An Account of the Kinetic Theory of Viscosity, Thermal Conduction and Diffusion in Gases* (Cambridge University Press, Cambridge, 1990).

[40] F. A. Williams, Spray combustion and atomization, Phys. Fluids **1**, 541 (1958).

[41] R. O. Fox, A quadrature-based third-order moment method for dilute gas-particle flows, J. Comput. Phys. **227**, 6313 (2008).

[42] S. Saha and M. Alam, Normal stress differences, their origin and constitutive relations for a sheared granular fluid, J. Fluid Mech. **795**, 549 (2016).

[43] M. M. Attarakih, C. Drumm, and H.-J. Bart, Solution of the population balance equation using the sectional quadrature method of moments (SQMOM), Chem. Eng. Sci. **64**, 742 (2009).

[44] E. Madadi-Kandjani and A. Passalacqua, An extended quadrature-based moment method with log-normal kernel density functions, Chem. Eng. Sci. **131**, 323 (2015).

[45] D. L. Marchisio, J. T. Pikturna, R. O. Fox, R. D. Vigil, and A. A. Barresi, Quadrature method of moments for population-balance equations, AIChE J. **49**, 1266 (2003).

[46] C. Yuan and R. O. Fox, Conditional quadrature method of moments for kinetic equations, J. Comput. Phys. **230**, 8216 (2011).

[47] E. Masi, O. Simonin, E. Riber, P. Sierra, and L. Y. M. Gicquel, Development of an algebraic-closure-based moment method for unsteady Eulerian simulations of particle-laden turbulent flows in very dilute regime, Int. J. Multiphase Flow **58**, 257 (2014).

[48] A. Kaufmann, M. Moreau, O. Simonin, and J. Helie, Comparison between Lagrangian and mesoscopic Eulerian modeling approaches for inertial particles suspended in decaying isotropic turbulence, J. Comput. Phys. **227**, 6448 (2008).

[49] M. H. Kasbaoui, R. G. Patel, D. L. Koch, and O. Desjardins, An algorithm for solving the Navier-Stokes equations with shear-periodic boundary conditions and its application to homogeneously sheared turbulence, J. Fluid Mech. **833**, 687 (2017).

[50] O. Desjardins, G. Blanquart, G. Balarac, and H. Pitsch, High order conservative finite difference scheme for variable density low Mach number turbulent flows, J. Comput. Phys. **227**, 7125 (2008).

[51] J. Capecelatro and O. Desjardins, An Euler-Lagrange strategy for simulating particle-laden flows, J. Comput. Phys. **238**, 1 (2013).

[52] P. J. Ireland and O. Desjardins, Improving particle drag predictions in Euler-Lagrange simulations with two-way coupling, J. Comput. Phys. **338**, 405 (2017).

[53] J. T. Jenkins and M. W. Richman, Plane simple shear of smooth inelastic circular disks: The anisotropy of the second moment in the dilute and dense limits, J. Fluid Mech. **192**, 313 (1988).

[54] X. Shen and Z. Warhaft, The anisotropy of the small scale structure in high Reynolds number ($R_\lambda \sim 1000$) turbulent shear flow, Phys. Fluids **12**, 2976 (2000).

[55] M. H. Kasbaoui, D. L. Koch, G. Subramanian, and O. Desjardins, Preferential concentration driven instability of sheared gas-solid suspensions, J. Fluid Mech. **770**, 85 (2015).

[56] S. Tavoularis, Asymptotic laws for transversely homogeneous turbulent shear flows, Phys. Fluids **28**, 999 (1985).

[57] F. A. de Souza, V. D. Nguyen, and S. Tavoularis, The structure of highly sheared turbulence, J. Fluid Mech. **303**, 155 (1995).

[58] A. A. Townsend, Entrainment and the structure of turbulent flow, J. Fluid Mech. **41**, 13 (1970).

[59] J. R. A. Pearson, The effect of uniform distortion on weak homogeneous turbulence, J. Fluid Mech. **5**, 274 (1959).

[60] M. M. Rogers and P. Moin, The structure of the vorticity field in homogeneous turbulent flows, J. Fluid Mech. **176**, 33 (1987).

[61] A. M. Savill, Recent developments in rapid-distortion theory, Annu. Rev. Fluid Mech. **19**, 531 (1987).

[62] J. C. Isaza and L. R. Collins, Effect of the shear parameter on velocity-gradient statistics in homogeneous turbulent shear flow, J. Fluid Mech. **678**, 14 (2011).

[63] K. A. Brucker, J. C. Isaza, T. Vaithianathan, and L. R. Collins, Efficient algorithm for simulating homogeneous turbulent shear flow without remeshing, J. Comput. Phys. **225**, 20 (2007).

[64] S. B. Pope, Turbulent flows, Meas. Sci. Technol. **12**, 2020 (2001).

[65] M. H. Kasbaoui, Clustering of heavy inertial aerosols in sheared flows, Ph.D. thesis, Cornell University, 2017.

[66] A. M. Ahmed and S. Elghobashi, Direct numerical simulation of particle dispersion in homogeneous turbulent shear flows, Phys. Fluids **13**, 3346 (2001).

[67] P. Gualtieri, F. Picano, and C. M. Casciola, Anisotropic clustering of inertial particles in homogeneous shear flow, J. Fluid Mech. **629**, 25 (2009).

[68] A. Aliseda, A. Cartellier, F. Hainaux, and J. C. Lasheras, Effect of preferential concentration on the settling velocity of heavy particles in homogeneous isotropic turbulence, J. Fluid Mech. **468**, 77 (2002).

[69] Y. Xu and S. Subramaniam, A multiscale model for dilute turbulent gas-particle flows based on the equilibration of energy concept, Phys. Fluids **18**, 033301 (2006).

[70] G. F. K. Tay, D. C. S. Kuhn, and M. F. Tachie, Effects of sedimenting particles on the turbulence structure in a horizontal channel flow, Phys. Fluids **27**, 025106 (2015).

[71] L. Zhao, H. I. Andersson, and J. J. J. Gillissen, Interphasial energy transfer and particle dissipation in particle-laden wall turbulence, J. Fluid Mech. **715**, 32 (2013).

[72] K. D. Squires and J. K. Eaton, Particle response and turbulence modification in isotropic turbulence, Phys. Fluids A **2**, 1191 (1990).